

**Fermi National Accelerator Laboratory**

**FERMILAB-TM-1984**

## **In Situ Calibration of the CMS HCAL Detector**

J. Freeman and W. Wu

*Fermi National Accelerator Laboratory  
P.O. Box 500, Batavia, Illinois 60510*

December 1996

## **Disclaimer**

*This report was prepared as an account of work sponsored by an agency of the United States Government. Neither the United States Government nor any agency thereof, nor any of their employees, makes any warranty, expressed or implied, or assumes any legal liability or responsibility for the accuracy, completeness, or usefulness of any information, apparatus, product, or process disclosed, or represents that its use would not infringe privately owned rights. Reference herein to any specific commercial product, process, or service by trade name, trademark, manufacturer, or otherwise, does not necessarily constitute or imply its endorsement, recommendation, or favoring by the United States Government or any agency thereof. The views and opinions of authors expressed herein do not necessarily state or reflect those of the United States Government or any agency thereof.*

## **Distribution**

*Approved for public release; further dissemination unlimited.*

# In Situ Calibration of the CMS HCAL Detector

J. Freeman, W. Wu

December 20, 1996

## Introduction

One serious challenge for hadron calorimeters is setting the absolute calibration. Electromagnetic calorimeters in a magnetic spectrometer have the momentum of electrons to calibrate against. In addition, at hadron colliders,  $Z \rightarrow ee$  supplies a narrow resonance to determine calibrations. No such well-measured processes have been available in the past for hadron calorimeters. In high energy collisions, high Pt hadrons are not normally isolated, rather appearing as part of jets. Contamination of the energy scale by unmeasured neutrals or by leakage from adjacent particles is always a concern.

There are low cross section processes that possess jets of well understood energy, for example a high pt  $Z$  recoiling off of a single jet. The high energy and luminosity of the LHC may supply enough of these events for quantities useful for calibration. In this paper we outline the possibility for doing in situ calibration using  $Z$  recoiling off of a jet events, and  $t$ - $\bar{t}$  events. We also comment on the more conventional possibilities of using muons and energy-flow to calibrate.

## CDF $Z + \text{Jet}$ Analysis

CDF has studied calibration using  $Z$  events where the  $Z$  recoils off of a jet, due to initial state radiation of a gluon (ref 1). In principle, the gluon jet should balance the  $Z$ . Since the  $Z$  is required to decay into leptons, the  $Z$  Pt is well measured. Thus the parton Pt that formed the jet is in principle known, and we can calibrate the calorimeter.

Figure 1 shows the scatter plot for Et jet vs Pt Z for 100 pb<sup>-1</sup> of CDF data. In this analysis, only one jet of Et > 10 GeV is allowed. There is a good correlation between the Z Pt and the jet Et. Table 1 shows the average fractional difference between the jet and the Z for Pt Z > 30 GeV. They conclude from this that they can determine the jet energy scale to about 5%.

Table 1: Fractional energy error for different jet cone sizes. CDF Results.

Jet Cone Size	Fractional Energy Error
0.4	1.7%
0.7	5.1%
1.0	2.7%

### CMS Z + Jet Analysis

We have started an analysis to study Z+1jet production at the LHC and see if this is a useful source of in situ calibration. An advantage at the LHC is the much higher production cross section ( 1.8nb at the LHC compared to 0.1nb at the Tevatron for production \* branching fraction into electron and muon channels.) A disadvantage at the LHC is the expected 30 min-bias events that will overlap the Z event.

We have used ISAJET 7.09 and SSCSIM to generate and simulate the Z+1jet events and the 30 min-bias events expected at 10 \*\*34 running. The model for min-bias events is ISAJET DIJET events, with Jet Pt > 2GeV. The detector is simulated by the SSCSIM program, modified to the details of CMS. (Ref 2). This simulation includes the effects of: the central magnetic field; finite energy resolution in the calorimeters; longitudinal and transverse shower development; e/h; cracks and limited eta coverage; and calorimeter eta-phi and depth segmentation. We also use an "ideal detector" simulation for comparison. This ideal detector only includes the effect of finite eta coverage and calorimeter eta-phi granularity.

The Z decay leptons were required to be in the eta range  $\text{Eta} < 2.6$ . Only one jet of  $\text{Et} > 40$  GeV was allowed. The (cross section \* efficiency) for these cuts is 0.24nb.

In one month of running at 10\*\*33, we expect to get 700K events, enough to supply a calibration. ( We consider the case of low luminosity running to see if the rates are adequate for the initial calibration.) Figure 2 shows the scatter plot of jet Et vs Z Et for these events, including the effect of the min-bias events. The jet cone size is 0.4. We see a good correlation. Figure 3 shows the ratio of Jet Et / Z Et for events the jet lands in the central region of the calorimeter,  $\text{eta} < 1.5$ . Figures 4 and 5 show similar results for jets in the HF, and HV regions. We have studied the effect of variation of cone size. Tables 2, 3, and 4 summarize the results for the HB, HF, and HV respectively. We see that at least for the central region, this signal can be useful for calibration of jet energy scale. At high luminosity, with a large number of min-bias events, its utility in the forward directions becomes more questionable.

Table 2: CMS HB Average (Jet Et-Zpt) / Z Et for different jet cone sizes.

Jet Cone Size	Jet Et Range	$\langle(\text{Jet Et} - Z \text{ Et}) / Z \text{ Et}\rangle$ No Min Bias	$\langle(\text{Jet Et} - Z \text{ Et}) / Z \text{ Et}\rangle$ with 30 Min Bias
0.4	50 - 70	-0.023	-0.32
0.4	70 - 90	-0.078	-0.06
0.4	>90	-0.10	-0.07
0.7	50 - 70	-0.22	-0.31
0.7	70 - 90	-0.07	-0.05
0.7	>90	-0.07	-0.02
1.0	50 - 70	-0.22	-
1.0	70 - 90	0.05	-
1.0	>90	0.03	0.14

Table 3: CMS HF Average (Jet Et-Zpt) / Z Et for different jet cone sizes.

Jet Cone Size	Jet ET Range	$\langle(\text{Jet Et} - Z \text{ Et}) / Z \text{ Et}\rangle$ No Min Bias	$\langle(\text{Jet Et} - Z \text{ Et}) / Z \text{ Et}\rangle$ with 30 Min Bias
0.4	50 - 70	0.07	-
0.4	70 - 90	-0.09	0.24
0.4	>90	-0.01	0.41
0.7	50 - 70	-0.10	-
0.7	70 - 90	0.09	0.11
0.7	>90	0.02	0.32
1.0	50 - 70	-0.13	-
1.0	70 - 90	0.08	-
1.0	>90	0.04	0.46

### Reconstructing $W \rightarrow jets$ in T-Tbar events

Another interesting process is t-tbar production. Here both top quarks decay into  $W + b$ . We require one  $W$  to decay leptonically. The high Pt lepton from this decay will provide our trigger. The other  $W$  decays into quarks that form jets. These 2 jets, which will reconstruct to the  $W$  mass, provide our means of calibration. To eliminate the combinatorial confusion, we require that both  $b$ 's are tagged by the micro-vertex detector.

CDF has already performed this analysis with their top event data set.(ref 3) In 100 pb-1 of data, there are 8 events that have the topology, Nr jets = 4, 2 b-tagged jets, and missing Et and a lepton Pt consistent with a  $W$ . 3 jets were required to have Et > 15 GeV while the 4th was > 8 GeV. Figure 6 shows the reconstructed mass of the 2 untagged jets in the

Table 4: CMS HV Average (Jet Et-Zpt) / Z Et for different jet cone sizes.

Jet Cone Size	Jet ET Range	$\langle(\text{Jet Et} - Z \text{ Et}) / Z \text{ Et}\rangle$ No Min Bias	$\langle(\text{Jet Et} - Z \text{ Et}) / Z \text{ Et}\rangle$ with 30 Min Bias
0.4	50 - 70	-0.16	-
0.4	70 - 90	-0.07	-
0.4	>90	-0.16	0.10
0.7	50 - 70	-0.16	-
0.7	70 - 90	-0.07	0.04
0.7	>90	-0.03	0.30
1.0	50 - 70	-0.17	-
1.0	70 - 90	0.016	-
1.0	>90	0.05	0.48

event. We see that the W mass is well determined, with a  $\sigma/\text{mean}$  of about 10%.

The cross sections are very attractive at the LHC. The T-Tbar production cross section at the Tevatron is 5pb. At the LHC it is 600pb. We assume a 15% efficiency for tagging both b's in the event, the expectation for the Run II CDF upgrade. In this case the overall efficiency\*branching ratio for detecting t-tbar into this channel is about 3%. Consequently, we expect about 45,000 double-tagged events of this topology after 1 month of running at  $10^{33}$ .

We simulate the B-tagging by assuming that we can perfectly reconstruct the b-quarks, and use the b-quark generated 4-vectors. No eta or Et cuts are placed on the b's.

We define a "standard set" of analysis cuts:

1.  $2 < N_r \text{ Jets} < 6$ , where the jet is required to have  $P_t > 20$ , and  $\text{abs}(\text{ETA}) < 1.5$
2.  $\text{abs}(\text{eta Jet } 1) < 1.5$   $\text{abs}(\text{eta Jet } 2) < 1.5$  where jets 1 and 2 are the 2 leading jets.
3.  $30 < P_t \text{ of jet1} < 100$   
 $30 < P_t \text{ of jet2} < 100$
4.  $dR \text{ (between b quark 1 and jet } i) > 0.6$   
 $dR \text{ (between b quark 2 and jet } i) > 0.6$
5.  $2.0 > dR \text{ (between JET1 and JET2)} > 0.5$   
 $0.25 < \text{Angle}(\text{jet1} - \text{jet2}) < 1.5$

6. We also define a "top mass window" cut for the reconstructed top mass of the (jet1\*jet2\*b) system,  $M_t$ :

$$165 < M_t < 185 \text{ (ideal detector)}$$

$$130 < M_t < 170 \text{ (realistic detector).}$$

We note that the simulated effects in the realistic detector tend to cause energy loss, and pull the reconstructed top mass downward.

We then attempt to reconstruct the mass of the top quark that the hadronically decaying  $W$  came from. We do not know which b-jet to use, so initially we randomly choose one b-jet to use. The event is rejected if the reconstruction falls outside the window.

Figure 7 shows the fractional resolution for the reconstructed mass as a function of jet cone size. We see a clear minimum at  $R=0.4$ . We will choose this cone size for the following analyses.

We now look at both b quarks combinations and select the reconstructed mass ( $M_t$ ) that lies inside the "top mass window".

Figure 8 shows the reconstructed mass distribution for the ideal detector and a jet cone size of  $R=0.4$ , with no min-bias event background. There is a very sharp  $W$  peak. Figure 9 shows the same distribution for the simulation of the realistic detector. Finally, figure 10 shows the realistic detector simulation where we include the effect of the min bias events.

## Muons

Isolated muons generate a well known energy deposition in the calorimeter and can be used for calibration. Issues to understand are the isolation of the muon, the contribution from the 30 underlying min-bias events, and the changing energy deposition as a function of muon momentum (relativistic rise). In addition, another problem with this scheme is that the muon deposits about 1 GeV in the calorimeter segment, ( corresponding to 350 MeV  $E_t$  at  $\theta = 30$  degrees), while interesting scales are at the multi-100 GeV region. Small absolute errors measuring the muon energy deposition correspond to large errors at the interesting jet energy scale.

Figure 11 shows the  $E_t$  (= energy for this  $E_t$ ) distribution for a tower at  $\eta=0$  due to the 30 min-bias events per crossing. The mean energy deposition is 30 MeV, with a very long tail. Therefore we expect that muon calibration can be seriously contaminated by the min-bias background, especially at large  $\eta$ .

Because of these difficulties, it is unclear how useful muons are for energy scale determination.

### Energy Flow

Relative calibration of different towers (or regions) of the HCAL can be attempted by studying energy flow in min-bias events. We believe this is an unsuitable strategy for calibration because:

- Absolute energy flow into a tower will depend on the instantaneous luminosity of the LHC when the event was logged. (changing number of min-bias events.)
- Non-physics related energy deposition (for example neutrons from quadrupole interactions, ...) may be at a level that would skew the result. Phi symmetry of energy deposition can be distorted by these non-physics energy depositions, including scraping, cosmic rays, ...
- Detectors of different technology can react to background (neutrons for instance) in very different manners. In these cases it is not clear that the average energy deposition should be even continuous across detector boundaries, let alone the same.

To illustrate the difficulties in understanding min-bias energy flow, consider figure 12, energy flow in CDF min-bias events. The complex structure is thought to be due to the above mentioned problems. In summary, we feel that using min bias events for calibration is a very dubious proposition.

### References

1. Study of Gluon Radiation and Jet Energy Scale Using Z+Jets and Photons+Jets, Soo-Bong Kim and Steve Vejcik, CDF Note number CDF3006, July 9, 1995
2. Missing Et + Jets Signals for Supersymmetry in the CMS Detector at the LHC, I. Gaines, et al., Fermilab-FN-642, June, 1996
3. Hadronic W Decays in B Tagged Top Candidates, R. Wilkinson and R. Hollebeek, CDF 3136, May 4, 1995.

## Figures

1. Scatter Plot of Jet Et vs Z Pt for 100 pb-1 of CDF data. Only one jet with Et > 10 GeV was allowed per event.
2. Scatter Plot of Jet Et vs Z Et for CMS. Only one jet with Et > 10 GeV was allowed per event.
3. Ratio of Jet Et to Z Et for jets in  $\text{Eta} < 1.5$  (HB) for events with only one jet of Et > 10 GeV. A) No Min Bias events. B) With 30 Min Bias events.
4. Ratio of Jet Et to Z Et for jets in (HF) for events with only one jet of Et > 10 GeV. A) No Min Bias events. B) With 30 Min Bias events.
5. Ratio of Jet Et to Z Et for jets in  $2.6 < \text{Eta} < 5$  (HV) for events with only one jet of Et > 10 GeV. A) No Min Bias events. B) With 30 Min Bias events.
6. Reconstructed mass of the 2 untagged jets in the CDF Top dataset of lepton, missing Et, 4 jets, with 2 jets B-tagged by the microvertex detector.
7. Fractional resolution for the reconstructed mass (in percent) as a function of jet cone size.
8. Reconstructed mass distribution for the ideal detector and a jet cone size of  $R=0.4$ , with no min-bias event background.
9. Reconstructed mass distribution for the realistic detector and a jet cone size of  $R=0.4$ , with no min-bias event background.
10. Reconstructed mass distribution for the realistic detector and a jet cone size of  $R=0.4$ , with min-bias event background.
11. Et distribution for a single tower at  $\text{eta}=0$  produced by the (30) min-bias events per crossing.
12. Et flow as a function of eta for W and min-bias events in the CDF detector.

### Z+1 Jet Data (Run 1A+1B, 100 pb<sup>-1</sup>)

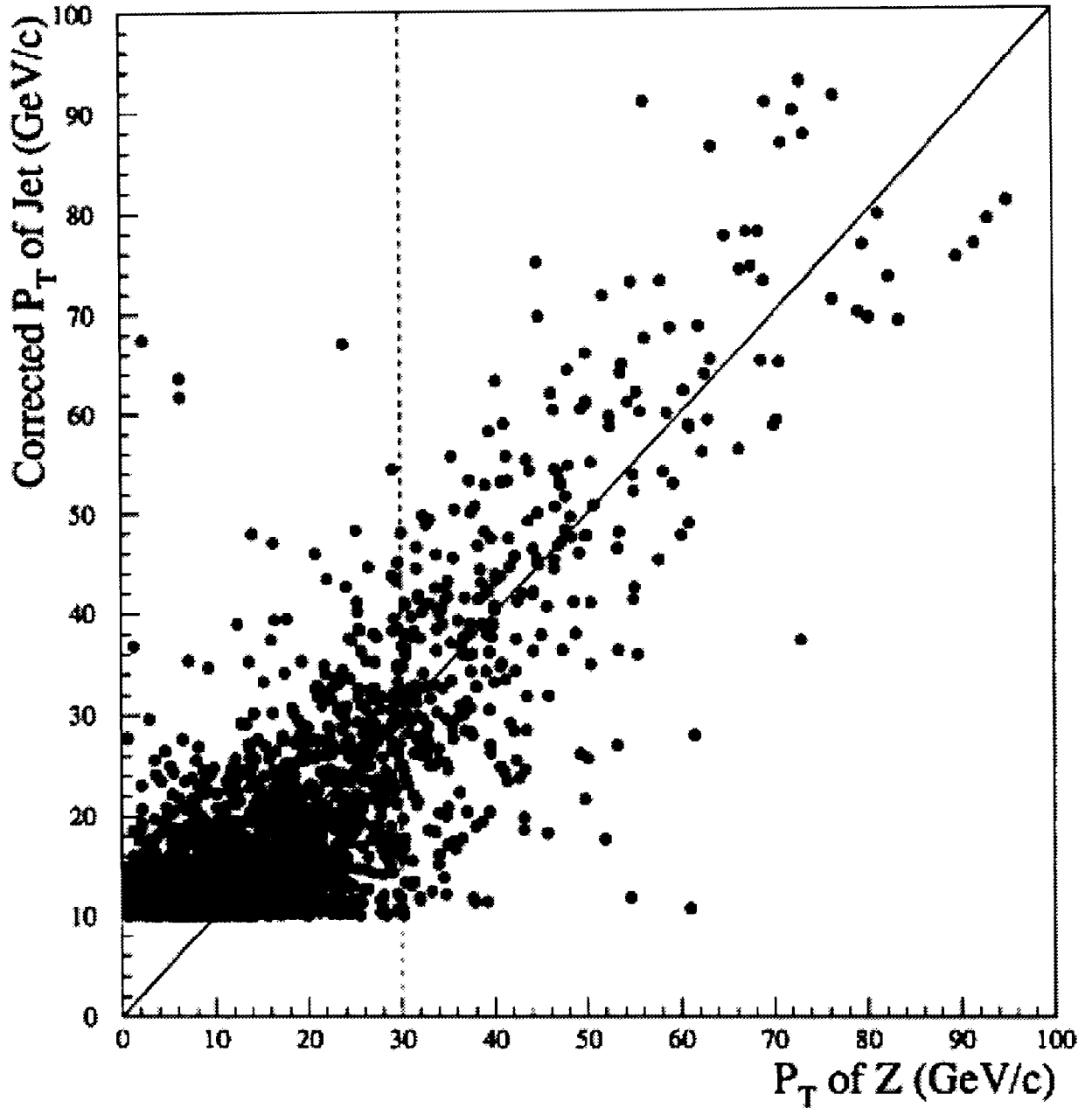


Figure 1: Scatter Plot of Jet Et vs Z Pt for 100 pb<sup>-1</sup> of CDF data. Only one jet with Et > 10 GeV was allowed per event.

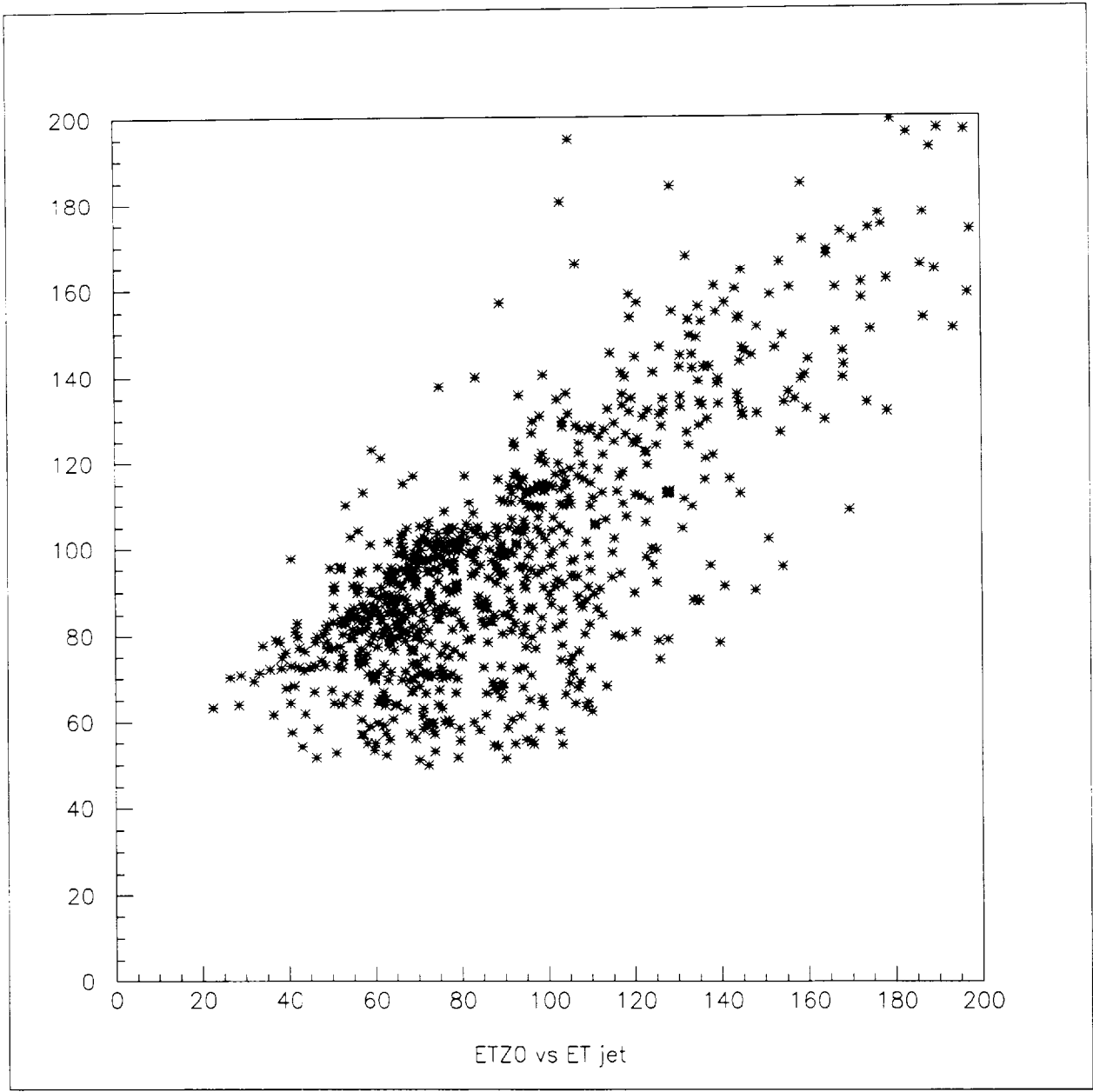


Figure 2: Scatter Plot of Jet Et vs Z Pt for CMS. Only one jet with  $E_t > 10$  GeV was allowed per event. 30 min-bias events per signal event are included.

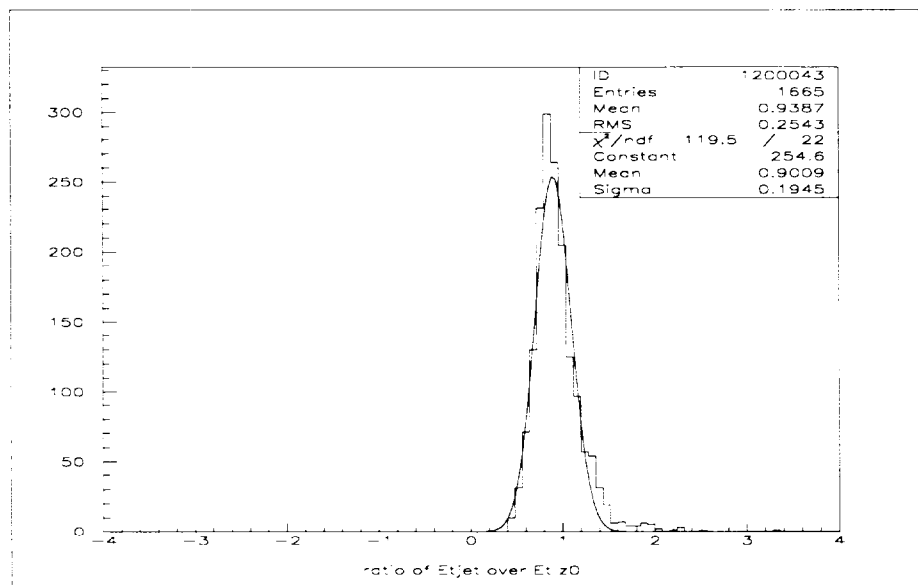
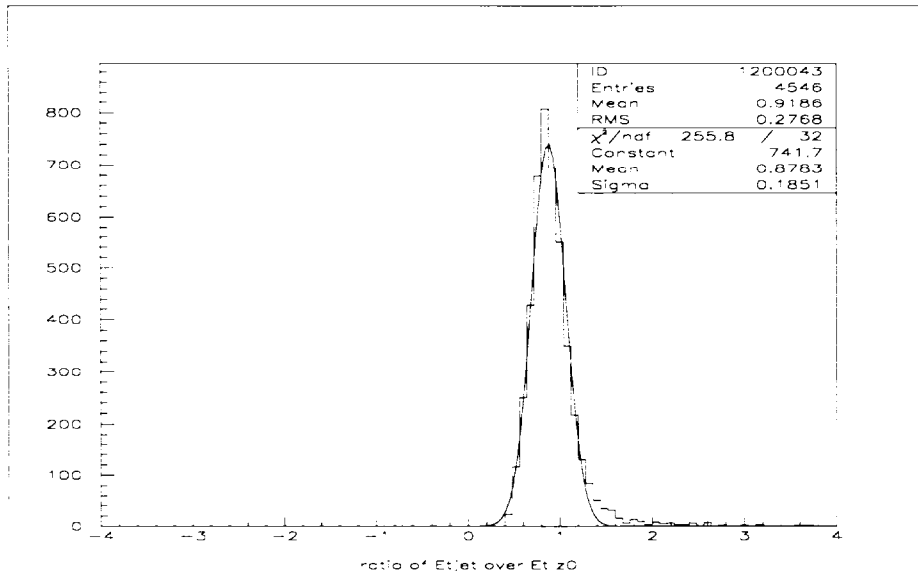


Figure 3: Ratio of Jet Et to Z Et for jets in  $\text{Eta} < 1.5$  (HB) for events with only one jet of  $\text{Et} > 10$  GeV. A) No Min Bias events. B) With 30 Min Bias events.

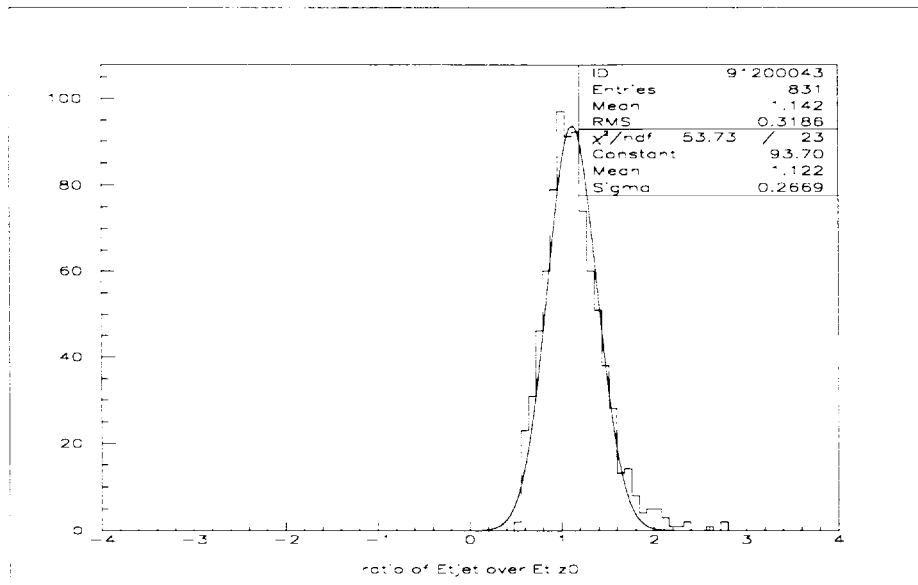
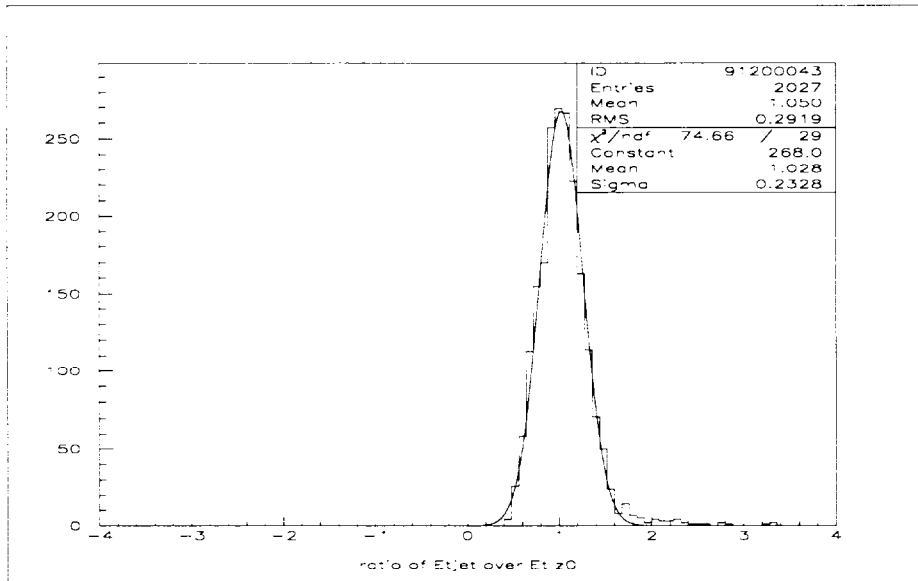


Figure 4: Ratio of Jet Et to Z Et for jets in (HF) for events with only one jet of Et > 10 GeV. A) No Min Bias events. B) With 30 Min Bias events.

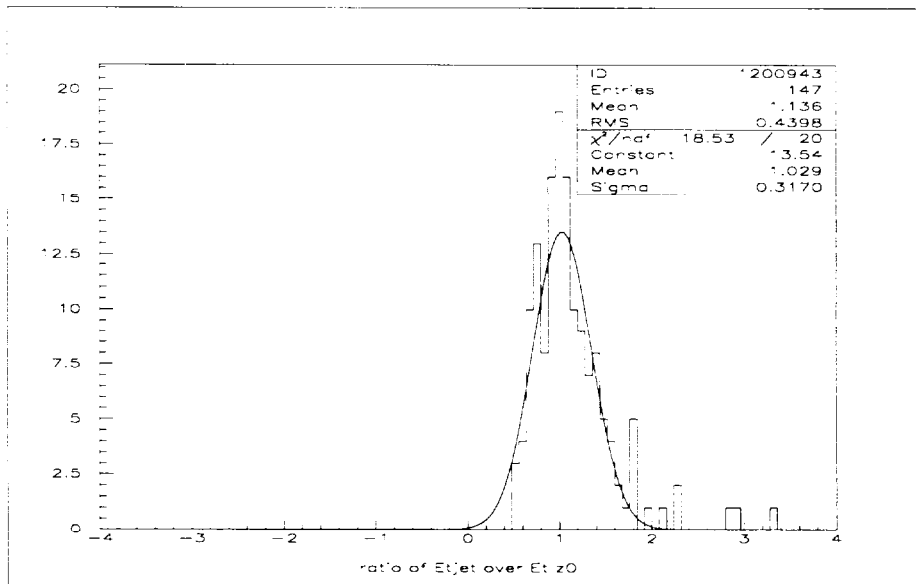
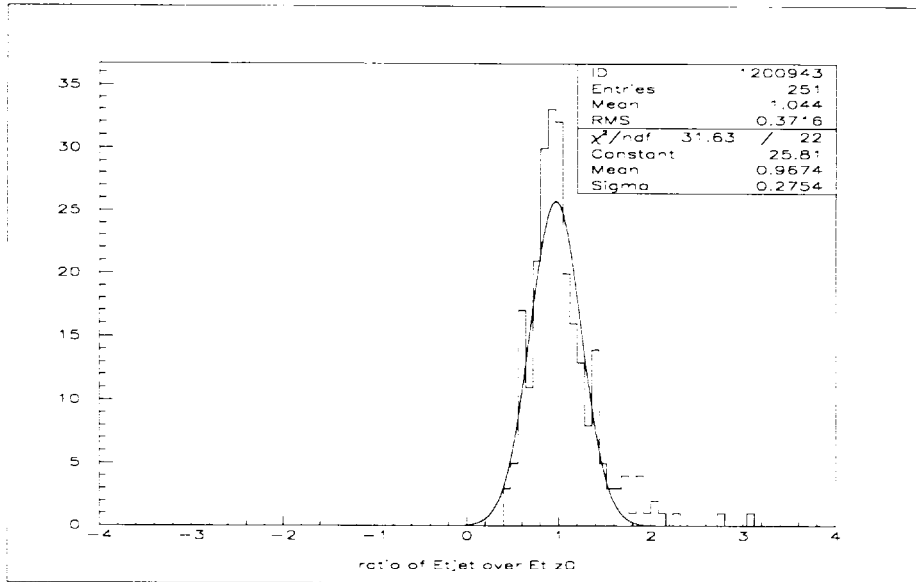


Figure 5: Ratio of Jet Et to Z Et for jets in  $2.6 < \text{Eta} < 5$  (HV) for events with only one jet of Et  $> 10$  GeV. A) No Min Bias events. B) With 30 Min Bias events.

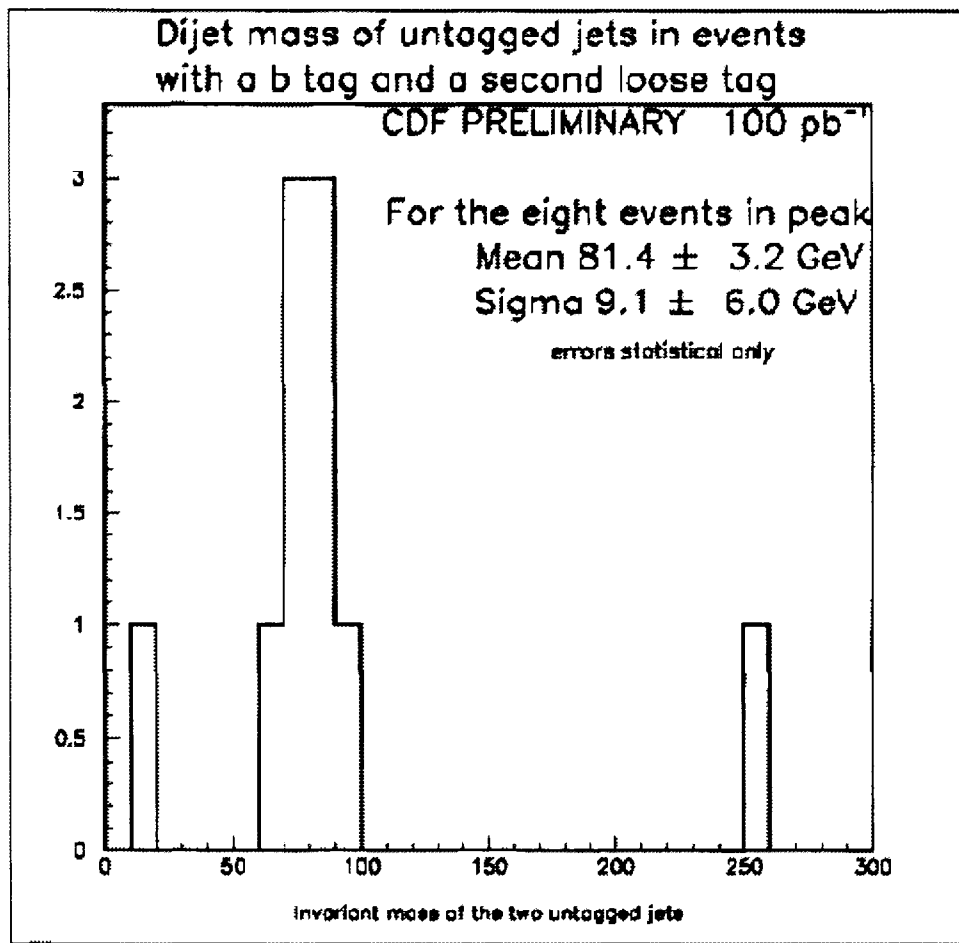


Figure 6: Reconstructed mass of the 2 untagged jets in the CDF Top dataset of lepton, missing  $E_t$ , 4 jets, with 2 jets B-tagged by the microvertex detector.

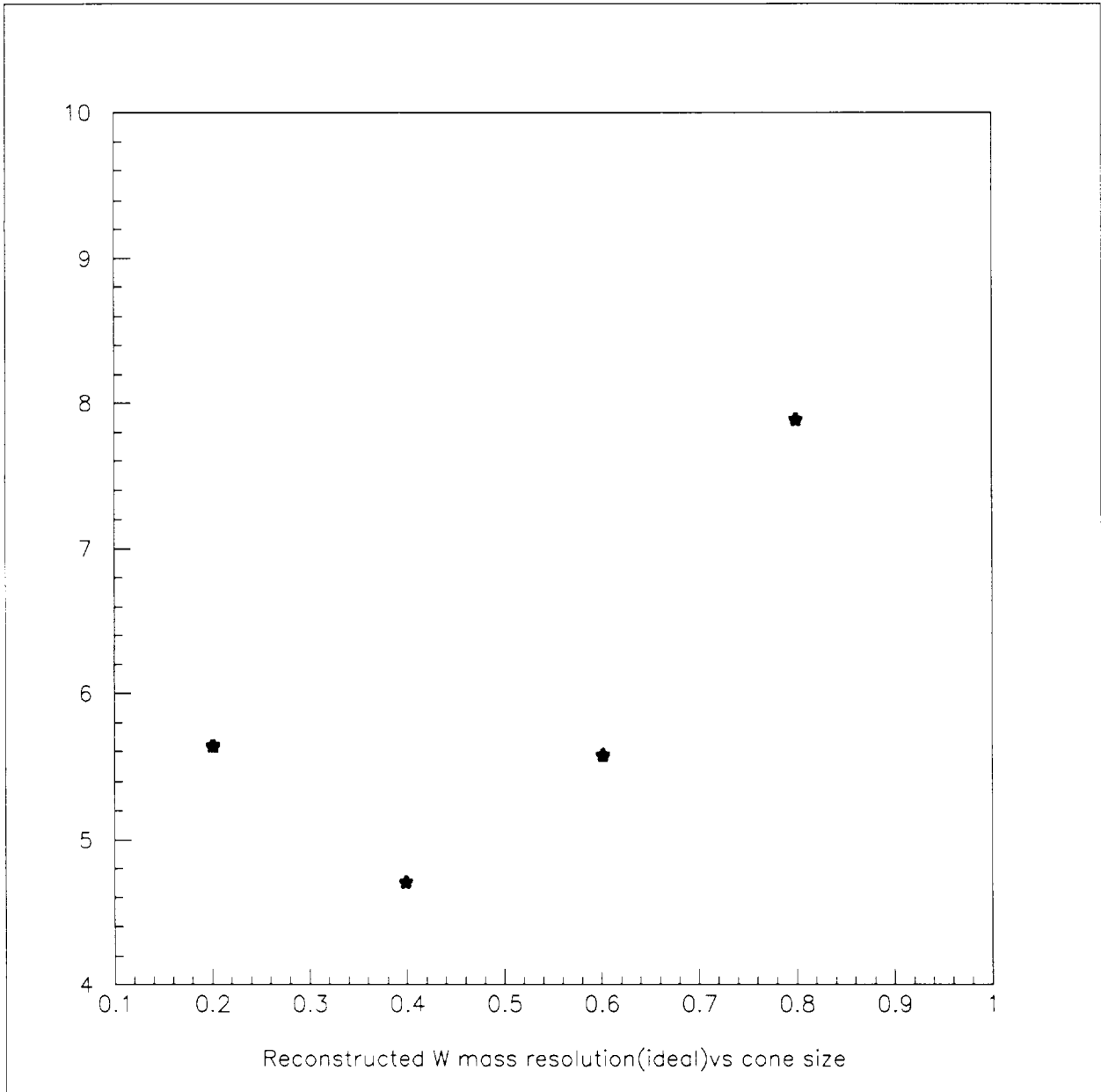


Figure 7: Fractional resolution for the reconstructed top mass (in percent) as a function of jet cone size.

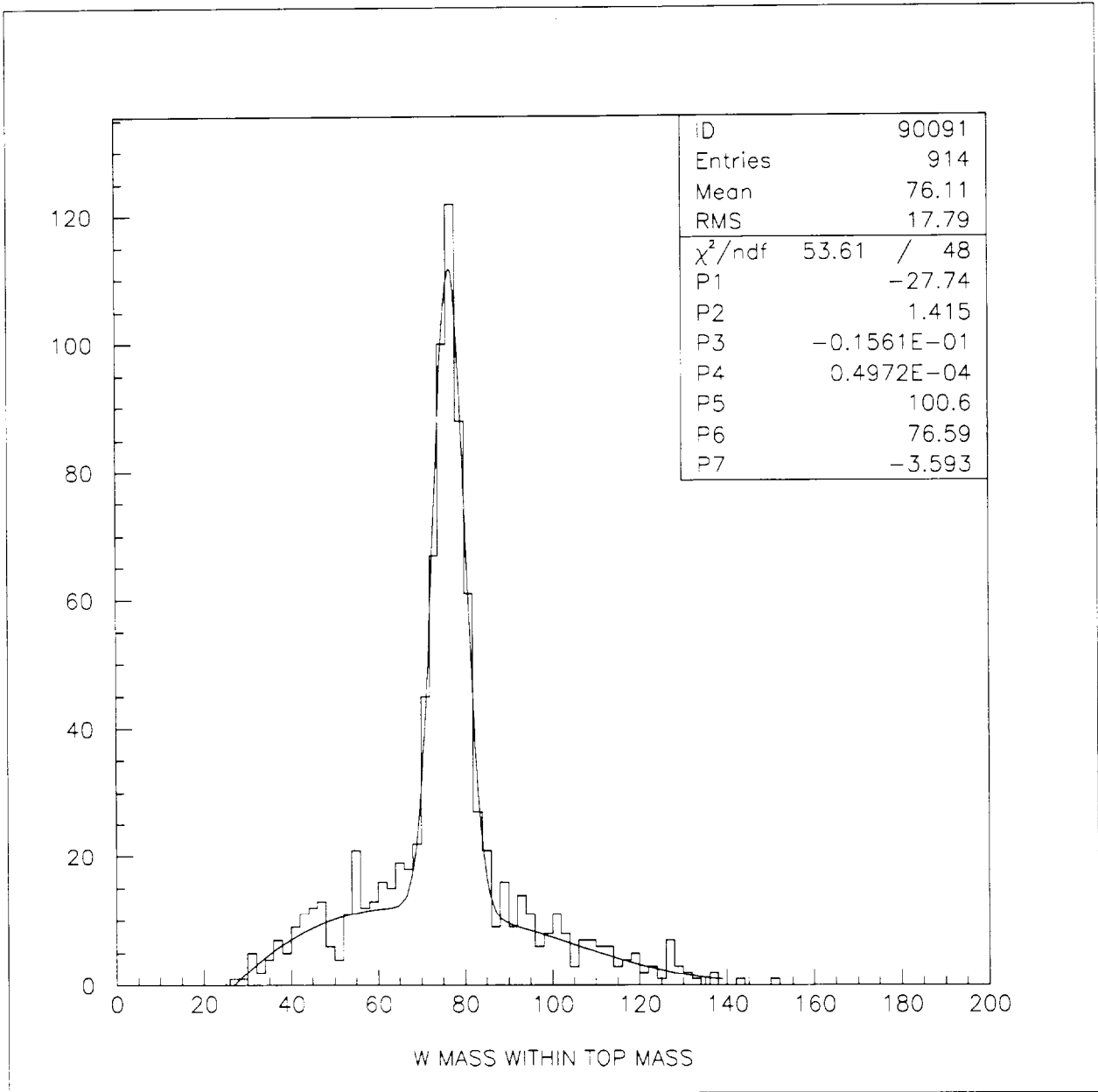


Figure 8: Reconstructed mass distribution for the ideal detector and a jet cone size of  $R=0.4$ , with no min-bias event background.

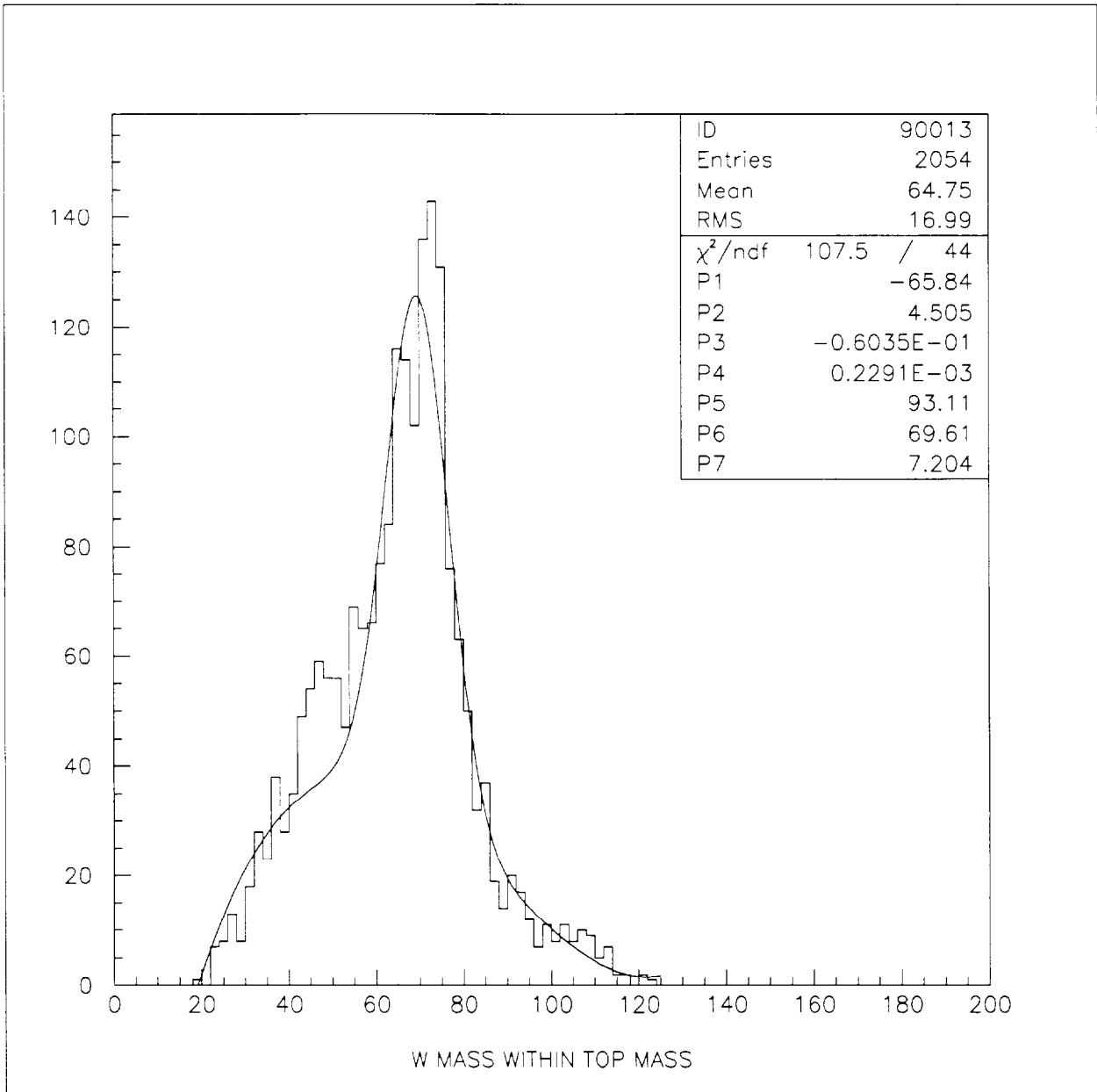


Figure 9: Reconstructed mass distribution for the realistic detector and a jet cone size of  $R=0.4$ , with no min-bias event background.

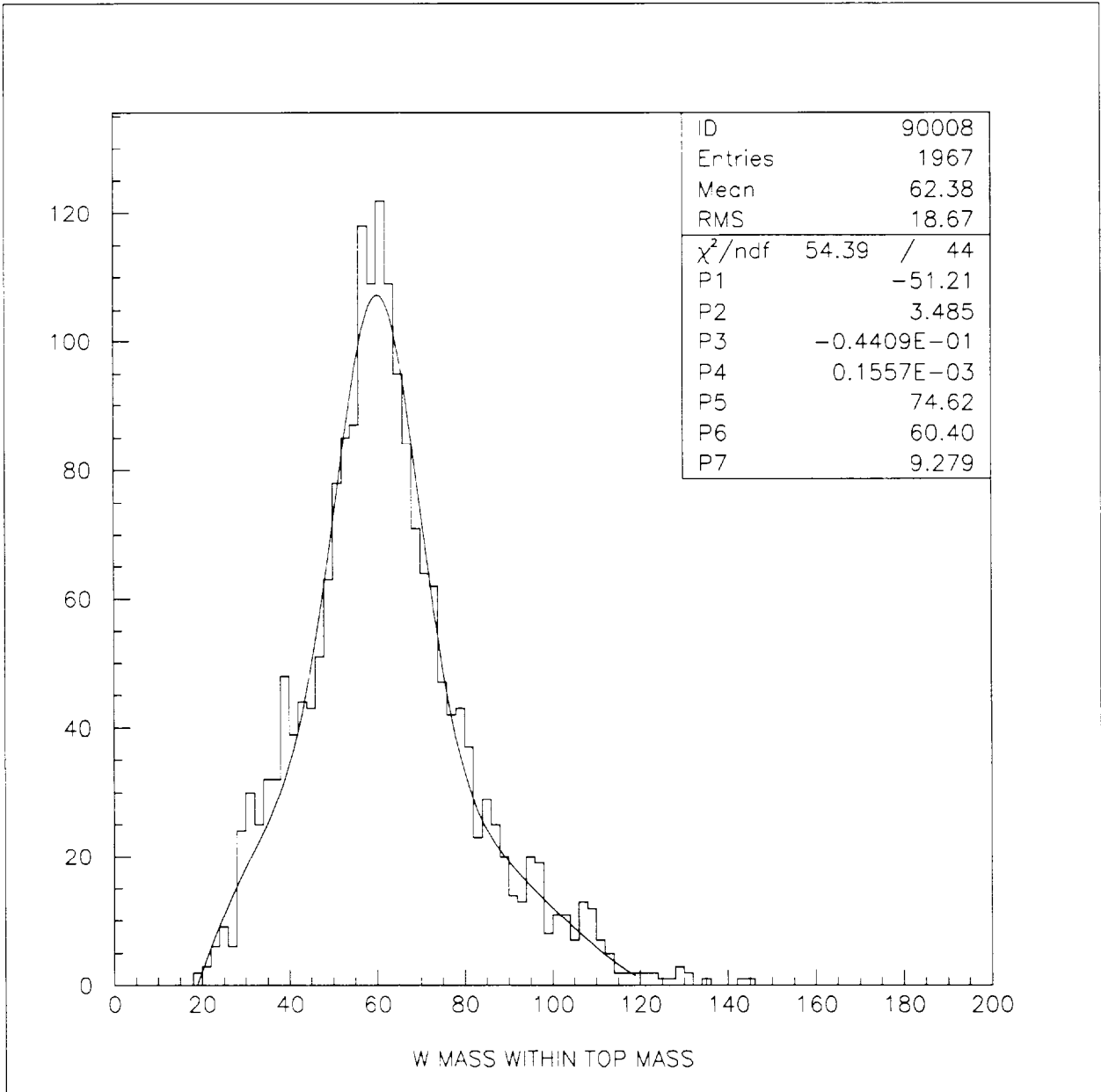


Figure 10: Reconstructed mass distribution for the realistic detector and a jet cone size of  $R=0.4$ , with min-bias event background.

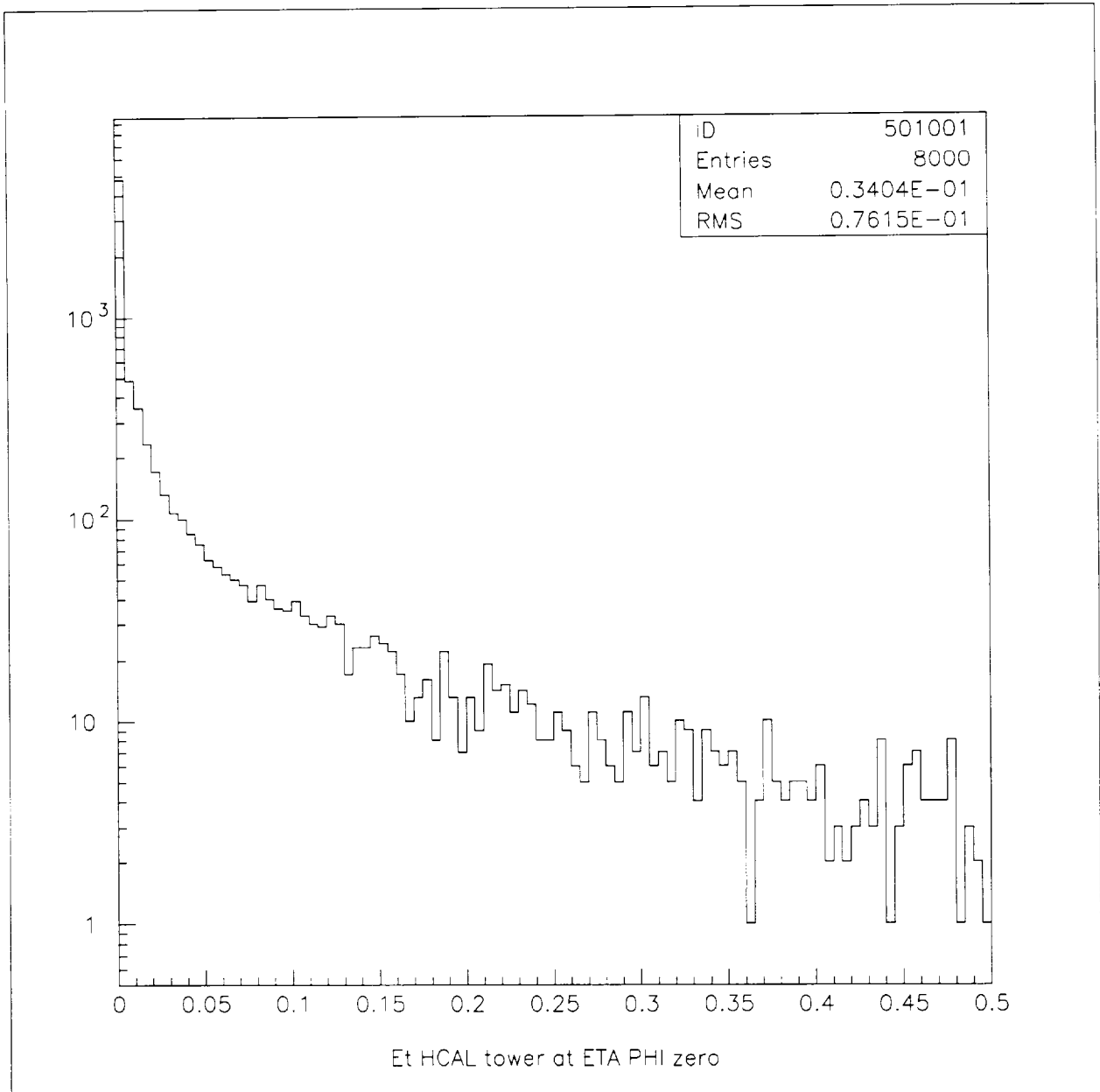


Figure 11: Et distribution for a single tower at eta=0 produced by the (30) min-bias events per crossing.

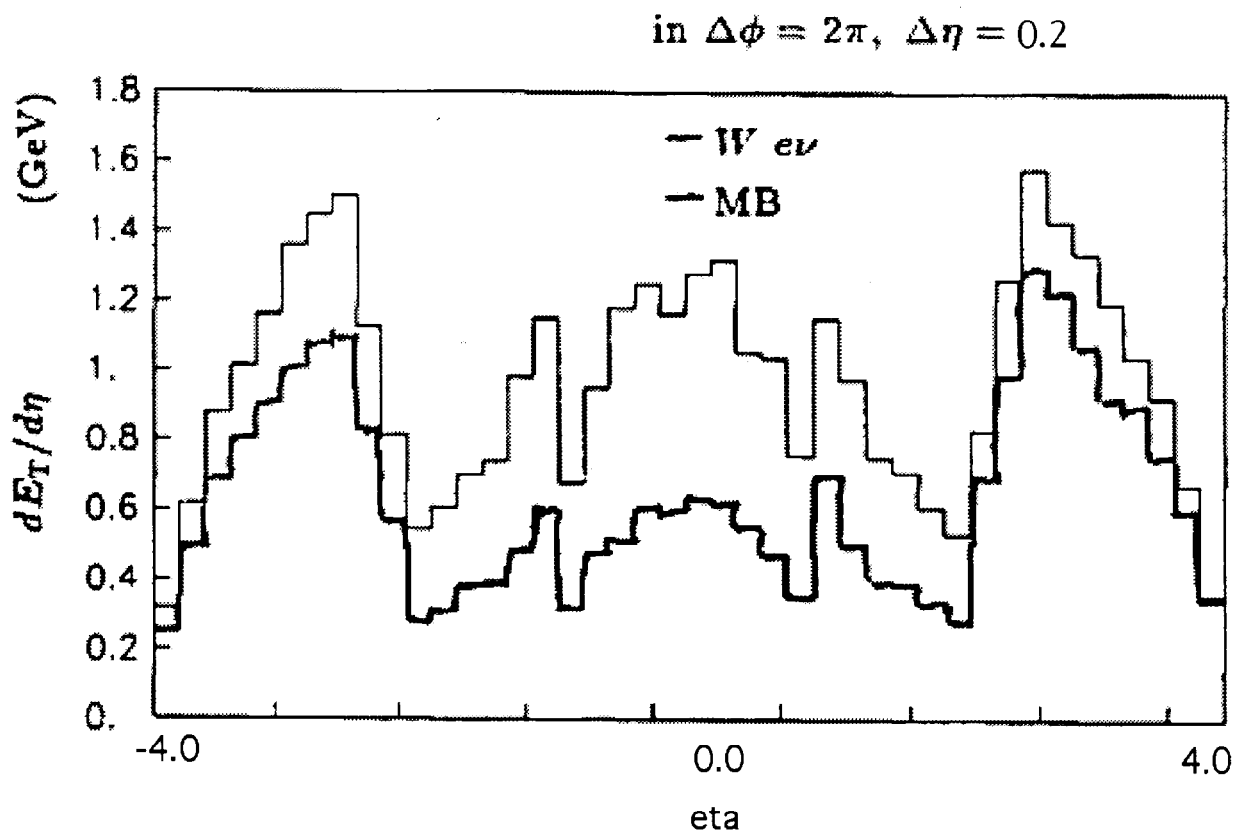


Figure 12: Et flow as a function of eta for W and min-bias events in the CDF detector.